Preprints of the 19th World Congress
The International Federation of Automatic Control
Cape Town, South Africa. August 24-29, 2014

Mass/Heat Transfer Enhancement Model for Boundary Layer Control Analysis

Ridwan Setiawan, Pesila Ratnayake and Jie Bao

School of Chemical Engineering
The University of New South Wales, Sydney NSW 2052, Australia
(email: j.bao@unsw.edu.au)

Abstract: Flow control has recently become an attractive technique to manipulate the behavior of fluid flow to achieve either mixing enhancement or the stabilization of turbulent flow. While it is understood that the location where mixing occurs is important, existing studies on mixing enhancement are limited to the hydrodynamics without considering the direct effect on mass/heat transfer improvement. This paper presents a reduced-order model for mass transfer equation which allows the analysis of the effect of an external actuation on mass transfer enhancement in a channel flow. When Reynolds number and temporal frequency of the external force are low, the effect of a forced wall slip velocity on the overall flow profile in a channel can be approximated by its instantaneous component. The estimated concentration profiles from the reduced-order model are in good agreement with CFD simulations. The key feature of the reduced-order model proposed in this paper is that it allows system analysis and control design to be performed by considering both spatial and temporal variables simultaneously.

Keywords: Modeling; Distributed Parameter Systems; Chemical Process Control

1. INTRODUCTION

Recent integration of different disciplines from control theory, fluid mechanics, Navier-Stokes mathematics to numerical methods has promoted flow control into an active area of research (Bewley [2001]). Flow control involves the manipulation of fluid flow into desired behavior commonly with the purpose to suppress turbulence or to enhance mixing. It may employ different control strategies, including active, passive, open-loop and closed-loop (Kim and Bewley [2007], Aamo and Krstić [2003]).

Aamo et al. [2003] presented the mixing enhancement through the application of feedback control on 2D channel boundary layer. The work has also been successfully extended to 3D pipe flow (Balogh et al. [2005]). It has been shown that by carefully controlling the flow system, mixing can be improved considerably using only small control effort realized by flow suction and injection across the wall. Furthermore, Schuster et al. [2008] studied the mixing enhancement of electrically conduction fluids moving in electromagnetic fields. The effect on heat transfer improvement of the fluids under electromagnetic field actuation was also presented (Luo and Schuster [2006]). However, existing mixing enhancement studies that utilize flow control only consider the fluid dynamics while excluding the underlying mass and heat transfer phenomena in the problem formulation. In most cases, fluid mixing enhancement does not translate to the same degree of mass and heat transfer improvement. Furthermore, ignoring the mass and heat transfer equations means that it is impossible to quantify the transfer enhancement directly.

The case where fouling reduction of membrane system operation in the laminar flow region motivates the investigation of the effect of flow control to mass transfer enhancement in a channel flow. As a membrane process operates, rejected substances in the feed accumulate near the feed side of the membrane and then form concentration polarization. This leads to the increased resistance to filtration, which reduces productivity and increases energy consumption. An external field method as a means to reduce concentration polarization and fouling has a potential for implementation because it can be applied independently of the velocity and membrane modifications (Nadh Jagannadh and Muralidhara [1996]). Applying an external field near a membrane surface can potentially disrupt the concentration boundary layer and enhance mass transfer (by increasing mixing) and therefore, reduce concentration polarization/fouling (Ouyang et al. [2013], Liang et al. [2014]).

In this paper, a reduced-order model (ROM) which combines the Navier-Stokes (NS) and mass transfer equations is presented. The model can simulate the effect of the externally applied forced wall slip velocity on the solute concentration response in a membrane channel flow. Furthermore, the ROM provides an explicit relationship between forced slip velocity and solute concentration, and therefore can be used for system analysis and has a potential to aid control design.

[1] This work is partially supported by ARC Discovery Project DP110101643

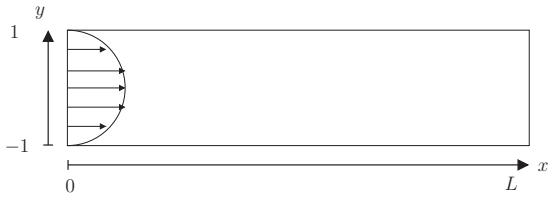

Fig. 1. 2D channel with developed parabolic velocity

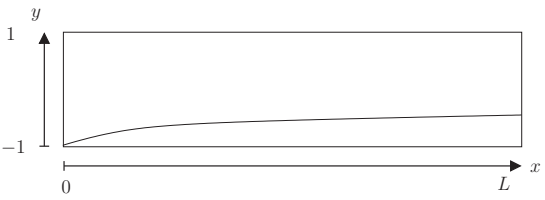

Fig. 2. 2D channel with developing concentration

2. SYSTEM DESCRIPTION

The system under consideration includes a 2D rectangular channel with a membrane installed on the lower wall. An ionic solution is fed into the channel at a constant rate which allows a steady-state flow to be developed in the channel. The system is described using impermeable-dissolving wall model, which provides a good approximation of the flow behavior and mass transfer in actual membrane systems without the need to explicitly model permeation (Fimbres Weihs et al. [2006]). The model assumes that the membrane side wall has constant solute concentration and the feed contains only solvent. For actuation, electrodes are installed below the membrane to generate an electric field that induces electro-osmotic flow, causing wall slip velocity in the stream-wise x-direction (Ouyang et al. [2013], Liang et al. [2014]). At equilibrium, a developed velocity profile (parabolic) and a developing solute concentration profile exist in the channel as illustrated in Fig. 1 and Fig. 2. Furthermore, the forced wall slip velocity acts as a perturbation to the system hence all of the systems are assumed to start from the steady-state condition.

3. MODELING AND ANALYSIS

3.1 Reduced-order Navier-Stokes Equations

For incompressible fluids with constant properties, the dimensionless linearized Navier-Stokes equations for a 2D channel flow are given as follows (Aamo and Krstić [2003]):

$$\frac{\partial^3\psi}{\partial t\partial y^2}+\frac{\partial^3\psi}{\partial t\partial x^2}+\tilde{U}\frac{\partial^3\psi}{\partial y^2\partial x}-\frac{\partial^2\tilde{U}}{\partial y^2}\frac{\partial\psi}{\partial x}+\tilde{U}\frac{\partial^3\psi}{\partial x^3}-\frac{4}{Re}\left(\frac{\partial^4\psi}{\partial x^4}+2\frac{\partial^4\psi}{\partial x^2\partial y^2}+\frac{\partial^4\psi}{\partial y^4}\right)=0, \tag{1}$$

where $\psi(x,y,t)$ is a single valued stream function such that

$$u(x,y,t)=\frac{\partial\psi}{\partial y}(x,y,t),\quad v(x,y,t)=-\frac{\partial\psi}{\partial x}(x,y,t),$$

and

$$(U,V)=\left(\frac{\hat{U}}{v_0},\frac{\hat{V}}{v_0}\right),\quad t=\frac{v_0}{l_0}\hat{t},$$
$$Re=\frac{4\rho l_0 v_0}{\mu},\quad (x,y)=\left(\frac{\hat{x}}{l_0},\frac{\hat{y}}{l_0}\right).$$

where (U,V) denotes the dimensionless velocity vector, t is the dimensionless time variable, and (x,y) is the dimensionless position vector. Re is the Reynolds number dependent on the fluid density (ρ), dynamic viscosity (μ), characteristic flow velocity v_0 (the average velocity of parabolic flow profile), and characteristic channel length l_0. In this paper, the discretization method requires that $0\le x\le L$ and $-1\le y\le 1$, such that $l_0=\hat{h}_{ch}/2$, where $\hat{h}_{ch}$ is the channel height. It should be noted that the length scale used in defining the Reynolds number is not the characteristic length l_0, but the hydraulic diameter (d_h), which is defined as 4 times the characteristic length ($d_h=4l_0$). Furthermore, the 'overhat' denotes actual variables.

Perturbation variables are used to study the effect of wall slip velocity to the hydrodynamics in the 2D channel:

$$u\triangleq U-\tilde{U},\ v\triangleq V-\tilde{V}, \tag{2}$$

with $(\tilde{U}=\frac{3}{2}(1-y^2),\tilde{V}=0)$ is the steady-state solution.

To obtain homogeneous boundary conditions, the following change of variables is performed

$$\phi(x,y,t)\triangleq\psi(x,y,t)-V_{12}(t)w(x)f(y) \tag{3}$$

where $V_{12}(t)=\frac{\hat{V}_{12}(t)}{\widetilde{V}_{12}}$ and $w(x)=\frac{\widetilde{V}_{12}\times\hat{w}(\hat{x})}{v_0}$ is the spatial field profile. $\widetilde{V}_{12}$ is defined as the base voltage, i.e. $\widetilde{V}_{12}=1$ Volt. $f(y)=\frac{1}{4}(y^3-y^2-y+1)$ is used to satisfy the boundary conditions, such that equation (1) becomes

$$\begin{aligned}&\frac{\partial^3\phi}{\partial t\partial y^2}+\frac{dV_{12}}{dt}w\frac{d^2f}{dy^2}+\frac{\partial^3\phi}{\partial t\partial x^2}+\frac{dV_{12}}{dt}\frac{d^2w}{dx^2}f\\&+\tilde{U}\left(\frac{\partial^3\phi}{\partial x\partial y^2}+V_{12}\frac{dw}{dx}\frac{d^2f}{dy^2}\right)-\frac{d^2\tilde{U}}{dy^2}\left(\frac{\partial\phi}{\partial x}+V_{12}\frac{dw}{dx}f\right)\\&+\tilde{U}\left(\frac{\partial^3\phi}{\partial x^3}+V_{12}\frac{d^3w}{dx^3}f\right)-\frac{4}{Re}\left[\left(\frac{\partial^4\phi}{\partial x^4}+V_{12}\frac{d^4w}{dx^4}f\right)\right.\\&\left.+2\left(\frac{\partial^4\phi}{\partial x^2\partial y^2}+V_{12}\frac{d^2w}{dx^2}\frac{d^2f}{dy^2}\right)+\left(\frac{\partial^4\phi}{\partial y^4}+V_{12}w\frac{d^4f}{dy^4}\right)\right]\\&=0,\end{aligned} \tag{4}$$

and boundary conditions in terms of ϕ are

$$\phi(x,y=1,t)=0,\quad \phi(x,y=-1,t)=0,$$
$$\frac{\partial\phi}{\partial y}(x,y=1,t)=0,\quad \frac{\partial\phi}{\partial y}(x,y=-1,t)=0.$$

3.2 Discretized Perturbation Navier-Stokes Equations

The Partial Differential Equation (PDE) is then discretized using the standard Fourier-Galerkin method in the stream-wise x-direction and the Chebyshev collocation method in the wall-normal y-direction. The Fourier-Galerkin method discretize x spatial domain into different wave numbers using a Fourier complex series as follows:

$$\phi(x,y,t) = \sum_{m=-M}^{M} a_m(y,t)P_m(x), \tag{5}$$

$$w(x) = \sum_{m=-M}^{M} w_m P_m(x), \tag{6}$$

where $P_m = e^{i\alpha_m x}$ and $\alpha_m = \frac{2\pi m}{L}$.

Because the PDE in (4) is linear, the Fourier-Galerkin discretization produces a set of equations which are decoupled in terms of wave number k, which can be decomposed into the real and imaginary parts of a_k (a_k^R and a_k^I). The discretization in the y-direction follows the Chebyshev collocation method on $N+1$ Chebyshev-Gauss-Labotto points defined as:

$$y_j = \cos\frac{\pi j}{N},\ j = 0,1,2,\ldots,N, \tag{7}$$

N should be chosen such that the details of the solute concentration boundary layer can be represented sufficiently using the discretization.

The boundary conditions of PDE (4) are then represented as:

$$\begin{aligned} a_k^R(y_0) = a_k^I(y_0) = a_k^R(y_N) = a_k^I(y_N) = 0 \\ a_k^R(y_1) = \mathbf{l}_1^T\bar{\mathbf{a}}^R,\ a_k^I(y_1) = \mathbf{l}_1^T\bar{\mathbf{a}}^I \\ a_k^R(y_{N-1}) = \mathbf{l}_2^T\bar{\mathbf{a}}^R,\ a_k^I(y_{N-1}) = \mathbf{l}_2^T\bar{\mathbf{a}}^I \end{aligned} \tag{8}$$

where

$$\begin{bmatrix}\mathbf{l}_1^T\\ \mathbf{l}_2^T\end{bmatrix} = -\begin{bmatrix} d_{01} & d_{0(N-1)} \\ d_{N1} & d_{N(N-1)}\end{bmatrix}^{-1}\begin{bmatrix} d_{02} & d_{03} & \cdots & d_{0(N-2)} \\ d_{N2} & d_{N3} & \cdots & d_{N(N-2)}\end{bmatrix}$$

and

$$\bar{\mathbf{a}}_k = [a_k(y_2)\ a_k(y_3)\ \cdots\ a_k(y_{N-2})]^T.$$

$$\mathbf{a}_k = \begin{bmatrix}\mathbf{0}^T\\ \mathbf{l}_1^T\\ \mathcal{I}_{N-3}\\ \mathbf{l}_2^T\\ \mathbf{0}^T\end{bmatrix}\bar{\mathbf{a}}_k = \mathcal{I}_a\bar{\mathbf{a}}_k,$$

with $\mathcal{D}_N \in \mathbb{R}^{(N+1)\times(N+1)}$ is the differentiation matrix defined as

$$(\mathcal{D}_N)_{jl} \triangleq d_{jl} = \begin{cases} \frac{\bar{c}_j}{\bar{c}_l}\frac{(-1)^{j+l}}{y_j - y_l} & j \neq l \\ -\frac{y_j}{2(1-y_j^2)} & 1 \le j = l \le N-1 \\ \frac{2N^2+1}{6} & j = l = 0 \\ -\frac{2N^2+1}{6} & j = l = N \end{cases} \tag{9}$$

and

$$\bar{c}_j = \begin{cases} 2 & j = 0 \text{ or } N \\ 1 & \text{otherwise}\end{cases} \tag{10}$$

The systems describing the dynamics of each wave number k can then be written in linear time invariant (LTI) state space form as follows:

$$\begin{bmatrix}\dot{\bar{\mathbf{a}}}_k^R\\ \dot{\bar{\mathbf{a}}}_k^I\end{bmatrix} = \bar{A}_{k,mod}\begin{bmatrix}\bar{\mathbf{a}}_k^R\\ \bar{\mathbf{a}}_k^I\end{bmatrix} + \bar{B}_{k,mod}\begin{bmatrix}V_{12}(t)\\ \frac{dV_{12}}{dt}\end{bmatrix} \tag{11}$$

where

$$\bar{A}_{k,mod} = \begin{bmatrix}\bar{M}^{-1}\bar{A}_R^R & \bar{M}^{-1}\bar{A}_R^I\\ \bar{M}^{-1}\bar{A}_I^R & \bar{M}^{-1}\bar{A}_I^I\end{bmatrix}$$

$$\bar{B}_{k,mod} = \begin{bmatrix}\bar{M}^{-1}(w_k^I\mathbf{q}_1 + w_k^R\mathbf{q}_2) & -w_k^R\bar{M}^{-1}\mathbf{g}\\ \bar{M}^{-1}(-w_k^R\mathbf{q}_1 + w_k^I\mathbf{q}_2) & -w_k^I\bar{M}^{-1}\mathbf{g}\end{bmatrix}$$

with

$$\begin{aligned} \bar{M} &= \bar{R}\left(\mathcal{D}_N^2 - \alpha_k^2\mathcal{I}\right)\mathcal{I}_a \\ \bar{R} &= \begin{bmatrix}\mathbf{0}_{(N-3\times 2)}\ \mathcal{I}_{N-3}\ \mathbf{0}_{(N-3\times 2)}\end{bmatrix} \\ \bar{A}_R^R &= \bar{A}_I^I = \frac{4}{Re}\bar{R}\left(\mathcal{D}_N^4\mathcal{I}_a - 2\alpha_k^2\mathcal{D}_N^2\mathcal{I}_a + \alpha_k^4\mathcal{I}_a\right) \\ \bar{A}_R^I &= -\bar{A}_I^R = \bar{R}\left(\alpha_k\tilde{U}_N\mathcal{D}_N^2\mathcal{I}_a - \left(\alpha_k\tilde{U}_N^{(2)} + \alpha_k^3\tilde{U}_N\right)\mathcal{I}_a\right) \\ \mathbf{q}_1 &= \bar{R}\left(\alpha_k\tilde{U}_N\mathbf{f}_N^{(2)} - \left(\alpha_k\tilde{U}_N^{(2)} + \alpha_k^3\tilde{U}_N\right)\mathbf{f}_N^{(0)}\right) \\ \mathbf{q}_2 &= \frac{4}{Re}\bar{R}\left(\alpha_k^4\mathbf{f}_N^{(0)} - 2\alpha_k^2\mathbf{f}_N^{(2)} + \mathbf{f}_N^{(4)}\right) \\ \mathbf{g} &= \bar{R}\left(\mathbf{f}_N^{(2)} - \alpha_k^2\mathbf{f}_N^{(0)}\right). \end{aligned} \tag{12}$$

and

$$\tilde{U}_N^{(r)} = \begin{bmatrix} \frac{d^r\tilde{U}}{dy^r}(y_0) & 0 & \cdots & 0 \\ 0 & \frac{d^r\tilde{U}}{dy^r}(y_1) & \cdots & 0 \\ \vdots & \vdots & \ddots & \vdots \\ 0 & 0 & \cdots & \frac{d^r\tilde{U}}{dy^r}(y_N)\end{bmatrix}, r = 0,1,2,\cdots$$

$$\mathbf{f}_N^{(r)} = \begin{bmatrix}\frac{d^r f}{dy^r}(y_0)\ \frac{d^r f}{dy^r}(y_1)\ \cdots\ \frac{d^r f}{dy^r}(y_N)\end{bmatrix}^T, r = 0,1,2,\cdots$$

From $\bar{\mathbf{a}}_k^R(t)$ and $\bar{\mathbf{a}}_k^I(t)$, the coefficients of the Fourier series expansion in (5) (i.e. $\phi(x,y,t) = \sum_{k=-M}^{M} a_k(y,t)P_k(x)$) are obtained. Hence, the perturbation velocities at location (x, y_j) can be evaluated from

$$u(x,y_j,t) = \frac{\partial\phi}{\partial y}(x,y_j,t) + V_{12}(t)w(x)\frac{df(y_j)}{dy}, \tag{13}$$

$$v(x,y_j,t) = -\frac{\partial\phi}{\partial x}(x,y_j,t) - V_{12}(t)\frac{dw(x)}{dx}f(y_j),. \tag{14}$$

The solution to ODE (11) is

$$\begin{bmatrix}\bar{\mathbf{a}}_k^R(t)\\ \bar{\mathbf{a}}_k^I(t)\end{bmatrix} = e^{\bar{A}_{k,mod}\,t}\int_0^t e^{\bar{A}_{k,mod}\,\tau}\bar{B}_{k,mod}\begin{bmatrix}V_{12}(\tau)\\ \frac{dV_{12}}{d\tau}\end{bmatrix}d\tau. \tag{15}$$

From equation (15), the values of $\bar{\mathbf{a}}_k^R(t)$ and $\bar{\mathbf{a}}_k^I(t)$ are the results of the multiplication between $e^{\bar{A}_{k,mod}\,t}$ and the integral term. Since $\bar{A}_{k,mod}$ is dependent on Re number (because A_R^R and A_I^I depend on Re, as shown in equation (12)), then the eigenvalues of $\bar{A}_{k,mod}$ are also dependent on Re number. A simple calculation can be performed to show that lower Re will result in more negative eigenvalues (real part) of $\bar{A}_{k,mod}$, which implies that for sinusoidal inputs (V_{12} and $\frac{dV_{12}}{dt}$), $\phi(x,y,t) = \sum_{k=-M}^{M} a_k(y,t)P_k(x)$ will decay faster to $\mathbf{0}$. Additionally, if the input to the system (11) (i.e. $\frac{dV_{12}}{dt}$) is small, then the values of $\bar{\mathbf{a}}_k^R(t)$ and $\bar{\mathbf{a}}_k^I(t)$ are also expected to be small. Therefore, for bulk flow with small Re numbers and low temporal frequency of input voltage, the first term on the RHS of equation (13) to (14) can be assumed to be

negligible in comparison to the instantaneous (second) term. It is then possible to approximate u and v in equations (13) and (14) as:

$$u(x,y,t) \simeq V_{12}(t)w(x)\frac{df(y)}{dy}, \tag{16}$$

$$v(x,y,t) \simeq -V_{12}(t)\frac{dw(x)}{dx}f(y). \tag{17}$$

3.3 Reduced-order Heat/Mass Transfer Equations

It has been shown in Section 3.2 that the perturbation velocity profile can be approximated using its instantaneous component. By exploiting this observation, the following section provides a novel representation that provides a direct link between a forced wall slip velocity and mass transfer enhancement. Unlike the reduced-order perturbation NS-equations which is linear, the reduced-order mass transfer equation still exhibits input nonlinearity due to the non-spatially uniform solute concentration. Therefore, the extension of the discretization method from NS-equations to mass transfer equation is not trivial.

For the case of developing concentration boundary layer, the dimensionless solute concentration can be defined as:

$$Y = \frac{\hat{Y} - Y_0}{Y_w - Y_0} \tag{18}$$

where $\hat{Y}$ is actual concentration (mass fraction), Y_0 is the concentration at inlet and Y_w is the concentration on the lower wall. The dissolving wall dimensionless mass transfer equation is described as follows (Bird et al. [2002]):

$$\frac{\partial Y}{\partial t} + U\frac{\partial Y}{\partial x} + V\frac{\partial Y}{\partial y} = \frac{4}{Pe}\left(\frac{\partial^2 Y}{\partial x^2} + \frac{\partial^2 Y}{\partial y^2}\right), \tag{19}$$

where Pe is the Peclet number and $Pe = ReSc$ ($Sc = \frac{\mu}{\rho D_{AB}}$ is the Schmidt number), D_{AB} is the diffusivity coefficient of the solute to the bulk solution.

Suppose that $(\tilde{U}, \tilde{V} = 0, \tilde{Y})$ is the steady-state solution to the mass transfer equation (19) and $\omega \triangleq Y - \tilde{Y}$ is the mass fraction deviation variable. The simplified perturbation mass transfer equation is obtained by omitting the second order perturbation terms:

$$\frac{\partial \omega}{\partial t} + u\frac{\partial \tilde{Y}}{\partial x} + \tilde{U}\frac{\partial \omega}{\partial x} + v\frac{\partial \tilde{Y}}{\partial y} = \frac{4}{Pe}\left(\frac{\partial^2 \omega}{\partial x^2} + \frac{\partial^2 \omega}{\partial y^2}\right) \tag{20}$$

3.4 Discretized Perturbation Mass Transfer Equation

The mass transfer equation is discretized following the same method as for the Navier-Stokes equation. Consider the Fourier complex series

$$\begin{aligned}
\omega(x,y,t) &= \sum_{m=-M}^{M} b_m(y,t)P_m(x), \\
\frac{\partial \tilde{Y}}{\partial y}(x,y,t) &= \sum_{m=-M}^{M} s_m(y,t)P_m(x), \\
\frac{\partial \tilde{Y}}{\partial x}(x,y,t) &= \sum_{m=-M}^{M} r_m(y,t)P_m(x).
\end{aligned} \tag{21}$$

where $P_m = e^{i\alpha_m x}$ and $\alpha_m = \frac{2\pi m}{L}$. The two main difficulties in studying the effect of slip velocity to mass/heat transfer enhancement are equation (20) requires knowledge of the velocity profile at every location in the channel and the nonlinear input terms (i.e. $u\frac{\partial \tilde{Y}}{\partial x}$ and $v\frac{\partial \tilde{Y}}{\partial y}$) . However under certain conditions as discussed in Section 3.2 (laminar bulk flow and slow variation of perturbation signal), the perturbation hydrodynamics variables which affect the mass transfer are u and v can be approximated as (16) and (17), such that:

$$u\frac{\partial \tilde{Y}}{\partial x} = V_{12}(t)\frac{df(y)}{dy}\sum_{m=-M}^{M}\sum_{m=p+q} w_p r_q(y,t)P_m(x) \tag{22}$$

$$v\frac{\partial \tilde{Y}}{\partial y} = -V_{12}(t)f(y)\sum_{m=-M}^{M}\sum_{m=p+q} \alpha_p i w_p s_q(y,t)P_m(x) \tag{23}$$

Equation (20) can be written in separate wave number k as follows:

$$\begin{aligned}
\frac{\partial b_k}{\partial t} = &-\tilde{U}\alpha_k i b_k + \frac{4}{Pe}\frac{\partial^2 b_k}{\partial y^2} - V_{12}(t)\frac{df(y)}{dy}\sum_{k=p+q} w_p r_q(y,t) \\
&+ V_{12}(t)f(y)\sum_{k=p+q}\alpha_p i w_p s_q(y,t) - \frac{4}{Pe}\alpha_k^2 b_k.
\end{aligned} \tag{24}$$

For the dissolving wall model, the boundary conditions for the PDE (20) are represented as:

$$\begin{aligned}
b_k^R(y_0) = \mathbf{l}_3^T\bar{\mathbf{b}}_k^R,\ b_k^I(y_0) = \mathbf{l}_3^T\bar{\mathbf{b}}_k^I \\
b_k^R(y_N) = b_k^I(y_N) = 0
\end{aligned} \tag{25}$$

where

$$\mathbf{l}_3^T = -d_{00}^{-1}\begin{bmatrix} d_{01} & d_{02} & \cdots & d_{0(N-1)}\end{bmatrix}$$

and

$$\bar{\mathbf{b}}_k = \left[b_k(y_1)\ b_k(y_2)\ \cdots\ b_k(y_{N-1})\right]^T.$$

$$\mathbf{b}_k = \begin{bmatrix} \mathbf{l}_3^T \\ \mathcal{I}_{N-1} \\ \mathbf{0}^T \end{bmatrix}\bar{\mathbf{b}}_k = \mathcal{I}_b\bar{\mathbf{b}}_k.$$

For each wave number k, the real and imaginary parts of equation (24) can then be written in a linear time invariant (LTI) state space form as follows:

$$\begin{bmatrix}\dot{\bar{\mathbf{b}}}_k^R \\ \dot{\bar{\mathbf{b}}}_k^I\end{bmatrix} = A_k\begin{bmatrix}\bar{\mathbf{b}}_k^R \\ \bar{\mathbf{b}}_k^I\end{bmatrix} + B_k V_{12}(t) \tag{26}$$

where

$$A_k = \begin{bmatrix} M^{-1}A_R^R & M^{-1}A_R^I \\ M^{-1}A_I^R & M^{-1}A_I^I \end{bmatrix},$$

$$B_k = \begin{bmatrix} -M^{-1}R\left(\mathbf{f}_N^{(1)}\sum_{k=p+q}\left(w_p^R r_q^R - w_p^I r_q^I\right)\right) \\ -M^{-1}R\left(\mathbf{f}_N^{(1)}\sum_{k=p+q}\left(w_p^R r_q^I + w_p^I r_q^R\right)\right)\end{bmatrix}$$

$$+ \begin{bmatrix} -M^{-1}R\left(\mathbf{f}_N^{(0)}\sum_{k=p+q}\alpha_p\left(w_p^R s_q^I + w_p^I s_q^R\right)\right) \\ -M^{-1}R\left(\mathbf{f}_N^{(0)}\sum_{k=p+q}\alpha_p\left(w_p^I s_q^I - w_p^R s_q^R\right)\right)\end{bmatrix}$$

with

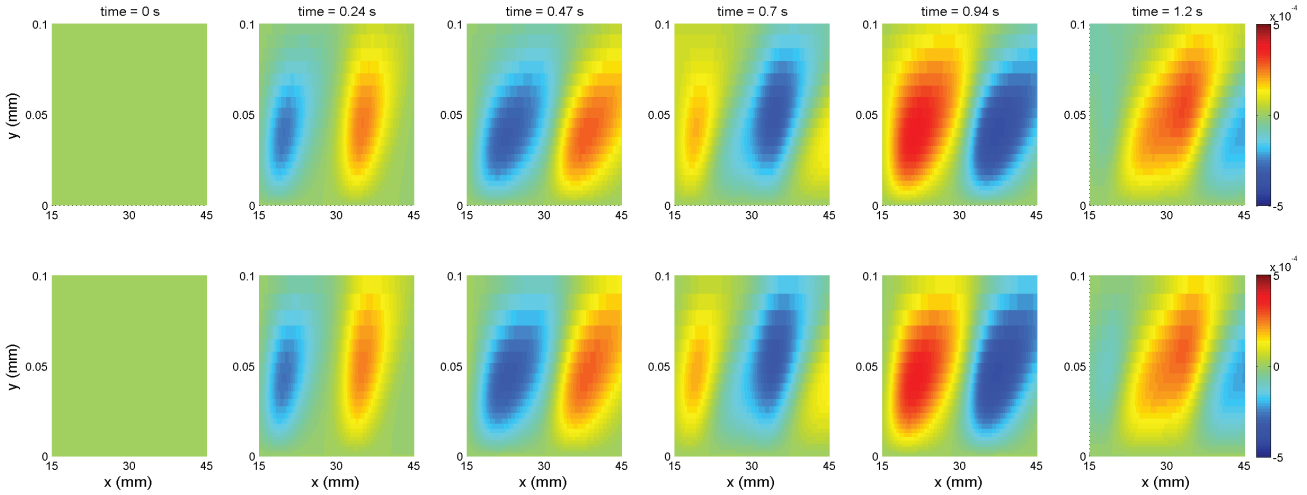

Fig. 3. Mass transfer model and CFD simulations (top model, bottom CFD) $Re = 280$

$$
\begin{aligned}
M &= R\mathcal{I}_b \\
R &= \left[\mathbf{0}_{(N-1\times 1)}\ \mathcal{I}_{N-1}\ \mathbf{0}_{(N-1\times 1)}\right] \\
A_R^R &= A_I^I = \frac{4}{Pe} R\left(\mathcal{D}_N^2 - \alpha_k^2 \mathcal{I}\right)\mathcal{I}_b \\
A_R^I &= -A_I^R = R\left(\alpha_k \tilde{U}_N \mathcal{I}_b\right)
\end{aligned}
$$

Fig. 3 shows that the simulation results obtained from the LTI mass transfer model and Computational Fluid Dynamics (CFD) are in good agreement with a reasonably shorter computational time (approximately 1 to 20).

The mass transfer equation (26) is extended to allow further investigation on the effect of u_s to mass transfer enhancement by allowing each wave number of the velocity $u(\alpha_p)$ to be adjusted independently such that $w_p V_{12}(t) = w_p(t)$ such that

$$
\begin{bmatrix} \dot{\bar{\mathbf{b}}}_k^R \\ \dot{\bar{\mathbf{b}}}_k^I \end{bmatrix} = A_k \begin{bmatrix} \bar{\mathbf{b}}_k^R \\ \bar{\mathbf{b}}_k^I \end{bmatrix} + B_{k,ext}\mathbf{u} \tag{27}
$$

where

$$
A_k = \begin{bmatrix} M^{-1}A_R^R & M^{-1}A_R^I \\ M^{-1}A_I^R & M^{-1}A_I^I \end{bmatrix}
$$

$$
B_{k,ext} = \begin{bmatrix} -M^{-1}R\left(\mathrm{diag}(\mathbf{f}_N^{(1)})\mathbf{g}_{1u} + \mathrm{diag}(\mathbf{f}_N^{(0)})\mathbf{g}_{1v}\right) \\ -M^{-1}R\left(\mathrm{diag}(\mathbf{f}_N^{(1)})\mathbf{g}_{2u} + \mathrm{diag}(\mathbf{f}_N^{(0)})\mathbf{g}_{2v}\right) \end{bmatrix}
$$

$$
\mathbf{u} = \left[w_0^R(t)\ \cdots\ w_P^R(t)\ w_0^I(t)\ \cdots\ w_P^I(t)\right]^T
$$

$$
\mathrm{diag}(\mathbf{f}_N^{(r)}) = \begin{bmatrix} \frac{d^r f}{dy^r}(y_0) & 0 & \cdots & 0 \\ 0 & \frac{d^r f}{dy^r}(y_1) & \cdots & 0 \\ \vdots & \vdots & \ddots & \vdots \\ 0 & 0 & \cdots & \frac{d^r f}{dy^r}(y_N) \end{bmatrix}
$$

$$
\mathbf{g}_{1u} = \begin{bmatrix} \left(r_{k+0}^R + r_{k-0}^R\right) \\ \vdots \\ \left(r_{k+P}^R + r_{k-P}^R\right) \\ \left(r_{k+0}^I - r_{k-0}^I\right) \\ \vdots \\ \left(r_{k+P}^I - r_{k-P}^I\right) \end{bmatrix}^T, \mathbf{g}_{1v} = \begin{bmatrix} \alpha_0\left(-s_{k+0}^I + s_{k-0}^I\right) \\ \vdots \\ \alpha_P\left(-s_{k+P}^I + s_{k-P}^I\right) \\ \alpha_0\left(s_{k+0}^R + s_{k-0}^R\right) \\ \vdots \\ \alpha_P\left(s_{k+P}^R + s_{k-P}^R\right) \end{bmatrix}^T
$$

$$
\mathbf{g}_{2u} = \begin{bmatrix} \left(r_{k+0}^I + r_{k-0}^I\right) \\ \vdots \\ \left(r_{k+P}^I + r_{k-P}^I\right) \\ \left(-r_{k+0}^R + r_{k-0}^R\right) \\ \vdots \\ \left(-r_{k+P}^R + r_{k-P}^R\right) \end{bmatrix}^T, \mathbf{g}_{2v} = \begin{bmatrix} \alpha_0\left(s_{k+0}^R - s_{k-0}^R\right) \\ \vdots \\ \alpha_P\left(s_{k+P}^R - s_{k-P}^R\right) \\ \alpha_0\left(s_{k+0}^I + s_{k-0}^I\right) \\ \vdots \\ \alpha_P\left(s_{k+P}^I + s_{k-P}^I\right) \end{bmatrix}^T
$$

The wall slip velocity spatial profile in the x-direction for a given $u_s = V_{12}(t)w(x)$ is described by $w(x)$. If $w(x)$ is predetermined, then equation (26) allows the analysis of u_s in terms of the dynamical effect of $V_{12}(t)$ on the mass/heat transfer enhancement inside a 2D channel with a specific bulk flow. One major difference between the mass transfer LTI and the NS LTI equations is in the term which includes the convolution sum of wall slip velocity and equilibrium concentration (p and q for each k). This implies that nonlinearity of the inputs such that each wave number k of $w(x)$ affects not only the same k as in the Navier-Stokes case but all other k.

Based on (21) (for ω), solute concentration at different locations is a linear combination of the states in (26). A control law can then be easily designed to regulate concentration at those locations by manipulating wall slip velocity.

The extension of (26) to (27) has a threefold benefit: (1) the slip velocity profile is included as the system design parameter which can potentially optimize mass transfer instead of using a predetermined $w(x)$; (2) the system now has more manipulated variables $w_p(t)$ instead of the single variable $V_{12}(t)$. This implies that the model can be used for system design by selecting the optimum waveform and

the locations of actuators (e.g. electrodes); and (3) the predetermined profile $w(x)$ only allows a standing wave in the channel while the time-varying $w_p(t)$ can include moving waves.

3.5 Mass transfer enhancement analysis

In this paper, the mass transfer enhancement is defined as the oscillation amplitude of solute concentration in the boundary layer near the membrane surface (the lower wall). This measure is selected because oscillations of solute concentration in the boundary layer can potentially reduce concentration polarization and fouling. The proposed system analysis method is able to identify the temporal frequency which will cause the maximum amplitude of oscillation for a given input voltage $V_{12}(t)$. For the dissolving wall model, the steady-state solute concentration profile for the developing boundary layer can be described using an incomplete Gamma function (Doshi et al. [1971]) such that:

$$\begin{aligned}\frac{\partial \tilde{Y}}{\partial y}(x,y,t) &= -\left(\frac{9Pe}{4x}\right)^{\frac{1}{3}} \frac{e^{-\frac{(y+1)^3 Pe}{12x}}}{\Gamma(\frac{1}{3})},\\ \frac{\partial \tilde{Y}}{\partial x}(x,y,t) &= \left(\frac{Pe}{12x^4}\right)^{\frac{1}{3}} \frac{(y+1)e^{-\frac{(y+1)^3 Pe}{12x}}}{\Gamma(\frac{1}{3})}.\end{aligned} \tag{28}$$

Based on the LTI system in equation (26), the perturbation solute concentration at a specific location $\omega(x_i, y_j, t)$ can be calculated since the slip velocity profile $w(x)$, the steady-state flow, and the steady-state solute concentration profile are known. In order to obtain the system representation from $V_{12}(t)$ to $\omega(x_i, y_j, t)$, the system in (26) is rewritten as follows:

$$\begin{aligned}\dot{\bar{\mathbf{b}}} &= A\,\bar{\mathbf{b}} + BV_{12}(t)\\ \omega(x_i,y_j,t) &= C\,\bar{\mathbf{b}}\end{aligned} \tag{29}$$

where

$$A = \begin{bmatrix} A_1 & 0 & \cdots & 0\\ 0 & A_2 & \cdots & 0\\ \vdots & \vdots & \ddots & \vdots\\ 0 & 0 & \cdots & A_{M/2}\end{bmatrix}$$

$$B = \begin{bmatrix} B_1^T & B_2^T & \cdots & B_{M/2}^T\end{bmatrix}^T$$

$$C = \begin{bmatrix} C_1 & C_2 & \cdots & C_{M/2}\end{bmatrix}$$

$$C_k = \begin{bmatrix} \mathbf{0}_{(1\times j-1)} & 2\cos(\alpha_k x_i) & \mathbf{0}_{(1\times N-2)} & -2\sin(\alpha_k x_i) & \mathbf{0}_{(1\times N-1-j)}\end{bmatrix}$$

$$\bar{\mathbf{b}} = \begin{bmatrix} \bar{b}_1^{R^T} & \bar{b}_1^{I^T} & \cdots & \bar{b}_{M/2}^{R\ T} & \bar{b}_{M/2}^{I\ T}\end{bmatrix}^T.$$

The system then becomes single-input-single-output such that the temporal frequency response can be readily calculated.

4. CONCLUSION

This paper presents a reduced-order model which allows the analysis of the effect of wall slip velocity on mass transfer enhancement explicitly rather than the generic mixing enhancement. The model has shown a good agreement with CFD simulation results for bulk flows with low *Re* in 2D channels with slow time varying forced wall slip velocity. The proposed model is represented as a linear time invariant (LTI) system of different spatial wave numbers, which can be used for simulation, system analysis, and control design purposes.

The extended system in equation (27) assumes that the electrode configuration is arbitrary and the analysis will be able to identify not only the temporal frequency for maximum oscillation but also the spatial frequency (or the combinations of spatial frequencies). This means for a distributed parameter system, the system and control design in terms of actuator distributions and signal time variation of the controller outputs can be explicitly analyzed. However, studying the extended system will involve a 2D spatio-temporal frequency response analysis, which will be challenging due to the system's non-spatial invariant property.

REFERENCES

O. M. Aamo and M. Krstić. *Flow Control by Feedback: Stabilization and Mixing.* Springer-Verlag, London, 2003.

O. M. Aamo, M. Krstić, and T. R. Bewley. Control of mixing by boundary feedback in 2D channel flow. *Automatica*, 39:1597–1606, 2003.

A. Balogh, O. M. Aamo, and M. Krstić. Optimal mixing enhancement in 3-D pipe flow. *IEEE Transactions on Control Systems Technology*, 13:27–41, 2005.

T. R. Bewley. Flow control: new challenges for a new renaissance. *Progress in Aerospace Sciences*, 37:21–58, 2001.

R. B. Bird, W. E. Stewart, and E. N. Lightfoot. *Transport Phenomena.* John Wiley & Sons, Inc., New York, 2nd edition edition, 2002.

M. R. Doshi, A. K. Dewan, and W. N. Gill. The effect of concentration dependent viscosity and diffusivity on concentration polarization in reverse osmosis flow systems. *AIChE Symposium Series*, 68:323–339, 1971.

G. A. Fimbres Weihs, D. E. Wiley, and David F. Fletcher. Unsteady flow with mass transfer in narrow zigzag spacer-filled channels: A numerical study. *Industrial & Engineering Chemistry Research*, 45:6594–6603, 2006.

J. Kim and T. R. Bewley. A linear systems approach to flow control. *Annual Review of Fluid Mechanics*, 39: 383–417, 2007.

Y. Y. Liang, G. A. Fimbres Weihs, and D. E. Wiley. Approximation for modelling electro-osmotic mixing in the boundary layer of membrane systems. *Journal of Membrane Science*, 450:18–27, 2014.

L. Luo and E. Schuster. Heat transfer enhancement in 2D magnetohydrodynamic channel flow by boundary feedback control. In *Proceedings of the 45th IEEE Conference on Decision & Control, San Diego, CA*, 2006.

S. Nadh Jagannadh and H.S. Muralidhara. Electrokinetics methods to control membrane fouling. *Industrial & Engineering Chemistry Research*, 35:1133–1140, 1996.

H. Ouyang, J. Bao, G. A. Fimbres Weihs, and D. E. Wiley. Control study on mixing enhancement in boundary layers of membrane systems. *Journal of Process Control*, 23:1197–1204, 2013.

E. Schuster, L. Luo, and M. Krstić. Mhd channel flow control in 2D: Mixing enhancement by boundary feedback. *Automatica*, 48:2498–2507, 2008.